Article

Intensity Correlation Analysis on Blue-Violet Femtosecond Pulses from a Dispersion-Compensated GaInN Mode-Locked Semiconductor Laser Diode

Shunsuke Kono *, Rintaro Koda, Hideki Watanabe, Noriyuki Fuutagawa and Hironobu Narui

Compound Semiconductor Development Department, Semiconductor Device Development Division, Sony Corporation, 4-14-1 Asahi-cho, Atsugi-shi, Kanagawa 243-0014, Japan;
E-Mails: rintaro.koda@jp.sony.com (R.K.); hidekib.watanabe@jp.sony.com (H.W.); noriyuki.fuutagawa@jp.sony.com (N.F.); hironobu.narui@jp.sony.com (H.N.)

* Author to whom correspondence should be addressed; E-Mail: shunsuke.kono@jp.sony.com; Tel.: +81-50-3140-9782; Fax: +81-50-3809-1311.

Academic Editor: Malte C. Kaluza

Abstract: We investigated the spectral and temporal characteristics of blue-violet femtosecond optical pulses generated by a passively mode-locked GaInN laser diode in a dispersion-compensated external cavity. The output optical pulses at 400 nm were analyzed in detail by intensity auto- and cross-correlation measurements using second harmonic generation on the surface of a β-BaB$_2$O$_4$ crystal. The obtained results clarified wavelength-dependent chirp characteristics of the optical pulses. The analysis suggested that a large frequency shift due to saturation in the saturable absorber and gain sections played an important role in the generation of femtosecond optical pulses.

Keywords: GaN; mode-locked semiconductor laser diode; gain saturation; saturable absorption; self-phase modulation; soliton-like mode locking

1. Introduction

Ultrashort optical pulses are now widely applied in many fields of science and engineering. The high peak intensity of ultrashort optical pulses induces nonlinear optical effects, such as two-photon absorption, which enable the imaging of the three-dimensional structures of biological tissue [1].

Ultrashort duration of these optical pulses allows material processing while avoiding the effects of heat dissipation [2]. These applications are mostly based on commercially available mode-locked solid state or fiber lasers. Semiconductor laser diodes (LDs) offer advantages for generating ultrashort optical pulses due to their broad gain bandwidths. The use of direct electrical excitation allows the fabrication of compact and practical ultrashort laser pulse sources [3]. In particular, GaN-based semiconductors have a unique property, to generate photons in the blue-violet region [4,5]. This is a great advantage of nitride semiconductors since most solid state lasers require wavelength conversion in order to generate ultrashort optical pulses in this wavelength region.

We previously developed a blue-violet picosecond pulse laser, based on a GaN-based semiconductor LD [6]. Using a master oscillator power amplifier scheme, we succeeded in generating picosecond optical pluses of 2.2 nJ pulse energy [7]. The peak power was about 630 W, which is the highest so far reported for GaN-based LDs. The pulse energy is comparable to that of blue-violet optical pulses produced by frequency-doubled mode-locked Ti:Sapphire lasers.

In addition to developing a high power GaInN semiconductor optical amplifier (SOA), shortening the pulse duration is important for obtaining high-peak-power optical pulses, because the pulse energy available from SOAs is limited by the finite carrier lifetime. However, sub-picosecond optical pulses cannot be routinely generated using mode-locked semiconductor laser diodes (MLLDs). This is due to the strong coupling of the real and imaginary parts of the refractive index in the gain section of semiconductor LDs. In order to avoid this problem, a bisectional laser diode (BS-LD) using a quantum dot active layer was used to generate 390-fs optical pulses [8]. Intracavity dispersion compensation is another technique for reducing chirp in optical pulses from MLLDs. The use of MLLDs with dispersion-compensated external cavities was reported to increase the spectral bandwidth, but not to reduce the pulse duration. In these reports, femtosecond optical pulses were finally obtained only by compressing the optical pulses using dispersion-compensating optics [9].

Previously, we reported the generation of 200-fs optical pulses at 400 nm using a GaInN BS-LD in a dispersion-compensated external cavity, followed by spectral filtering [10,11]. With a negative intracavity group velocity dispersion (GVD), the output spectrum was broadened and optical pulses with a duration of 200 fs were produced by subsequent spectral filtering. There were three aspects of this situation that differed from previous reports of ultrashort pulse generation using dispersion-compensated MLLDs. First, ultrashort pulses close to the Fourier transform limit were obtained by spectral filtering. Second, the intracavity GVD was negative. Finally, the recovery time for the saturable absorber (SA) was as slow as 15 ps with a reverse bias voltage of 6 V [12]. These experimental conditions were similar to those for soliton mode locking with a slow SA [13]. However, in order to explain the femtosecond pulse generation mechanism in a GaInN MLLD in terms of soliton mode locking, it would be necessary for self-phase modulation to occur in order to balance the intracavity GVD. Furthermore, the theory of soliton mode locking cannot explain the shape of the optical pulses or the spectra of the GaInN MLLD before spectral filtering.

In the present study, we examined the temporal and spectral characteristics of optical pulses produced by a dispersion-compensated GaInN MLLD in order to clarify the pulse formation mechanism. For this purpose, we developed a cross-correlation measurement technique using second-harmonic generation (SHG) at the surface of a β-BaB$_2$O$_4$ (β-BBO) crystal. The remainder of this manuscript is organized as follows. Section 2 describes the experimental setup used in this study.

Section 3.1 reviews the results for femtosecond pulse generation by a GaInN MLLD in a dispersion-compensated external cavity. In Section 3.2, cross-correlation measurements are presented to clarify the true pulse shape and the spectro-temporal characteristics of the optical pulses. The results of the spectrally-resolved autocorrelation measurement are discussed in Section 3.3, in order to investigate the spectrally dependent chirp characteristics of the output optical pulses. On the basis of these experimental results, possible nonlinear optical effects responsible for pulse generation in GaInN MLLDs are discussed in Section 3.4.

2. Experimental Section

Figure 1 shows the experimental setup used in the present study [10,11]. A double-quantum-well GaInN BS-LD was operated in a dispersion-compensated external cavity under passive mode locking. The epitaxial structure of the device has previously been reported [14]. The p-electrode of the BS-LD had a gain section and an SA section. The device length was 600 μm and the SA length was 30 μm. The SA section was on the rear end of the device, and its facet had a high-reflection coating. The ridge waveguide was curved towards the output facet, which had an anti-reflection coating. The optical axis of the curved waveguide was slightly inclined with respect to the facet in order to reduce residual reflection. The external cavity had 4-*f* type dispersion-compensation optics, consisting of a diffraction grating (2400 grooves/mm) and a Fourier lens (f = 100 mm). An optical cavity was formed between the rear facet of the GaInN BS-LD and a folding mirror in the dispersion-compensation optics.
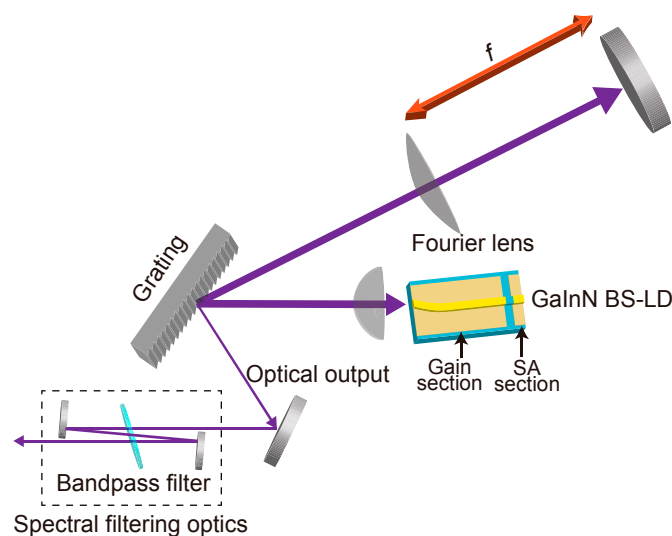

Figure 1. Schematic representation of dispersion-compensated GaInN MLLD including spectral filtering optics in order to obtain femtosecond optical pulses. Thick arrows represent the optical path of the external cavity configuration including GaInN BS-LD. The number of transmission through a bandpass filter was adjusted in order to obtain necessary bandwidth.

The output optical pulses were characterized using an optical spectrum analyzer (ANDO AQ-6315A), a microwave spectrum analyzer (Agilent, 8562EC) with fast photodiodes (NewFocus 1004, Thorlabs SV2), and a laboratory-made intensity autocorrelation measurement system [15]. This was based on SHG at the surface of a β-BBO crystal, because phase-matched SHG cannot be achieved

at 400 nm using commercially-available nonlinear optical crystals. Since the conversion efficiency of the surface SHG was as low as 10^{-7} with an input power of mW-order, frequency-resolved optical gating was not a practical means of characterizing the chirp characteristics of the output pulses.

3. Results and Discussion

3.1. Blue-Violet Femtosecond Pulse Generation by a GaInN MLLD

By varying the intracavity GVD, the ultrashort optical pulses from the GaInN MLLD changed drastically [10,11]. A typical intensity autocorrelation trace for output optical pulses from the MLLD with a negative intracavity GVD is shown as the blue trace in Figure 2a. The gain current was 140 mA and the reverse bias voltage applied to the SA section was 6.0 V. The average output power was about 12 mW and the pulse repetition rate was about 1 GHz. The intracavity GVD was estimated to be -0.058 ps^2 using the geometrical parameters of the dispersion-compensation optics. The blue trace in Figure 2b shows the corresponding optical spectrum. As reported previously, femtosecond optical pulses were obtained by extracting the short wavelength components of the optical spectrum. Figure 2a also shows an intensity autocorrelation trace for the optical pulses after the bandpass (BPF) filter (red trace). The spectral bandwidth of the BPF was 1.3 nm and the output beam was passed through the BPF twice in order to suppress the intense spectral components at longer wavelength. The resulting spectral width was 0.8 nm and the pulse duration was 210 fs, assuming a sech^2 function pulse shape. The time-bandwidth product was estimated to be 0.35, close to that of a Fourier transform limited pulse. The shortest pulse duration of 200 fs was obtained using another BPF of different spectral width [10]. The spectral components at the short wavelength edge of the optical spectrum were almost free from chirp. The average power after the BPF was about 0.8 mW. The pulse peak power was estimated to be about 4 W. The femtosecond pulse components were less than 10% of the total output power of the GaInN MLLD.
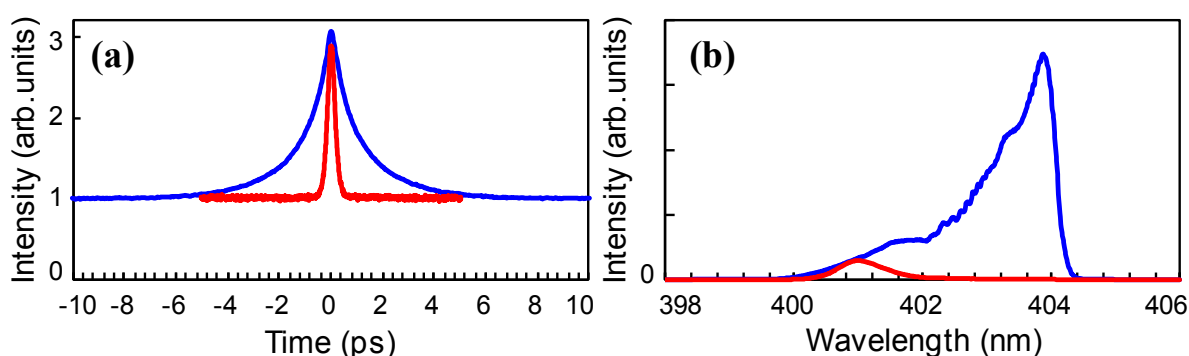

Figure 2. (**a**) Intensity autocorrelation traces for optical pulses from a GaInN MLLD with negative intracavity GVD measured without a bandpass filter (blue trace), and with a bandpass filter (red trace); (**b**) Corresponding optical spectra without a bandpass filter (blue trace), and with a bandpass filter (red trace).

3.2. Cross-Correlation Measurements of the Optical Pulses from a GaInN MLLD

The autocorrelation trace in Figure 2a shows that the output optical pulses from the GaInN MLLD without spectral filtering cannot be reproduced using either sech^2 or Gaussian function. The fact that the corresponding optical spectrum shown in Figure 2b is highly asymmetric suggests that the pulse shape was asymmetric in time. However, the intensity autocorrelation measurement provides only a symmetric time trace. In order to investigate the pulse characteristics, we used a cross-correlation technique. Since the femtosecond optical pulses were obtained by extracting the short wavelength edge of the optical spectrum, we can obtain cross-correlation signals between the direct optical output from the MLLD and the femtosecond optical pulses by inserting a BPF into one of the arms of the Michelson interferometer in the intensity autocorrelation setup, as shown in Figure 3a [10]. Figure 3b shows an example of cross correlation of the output optical pulses. The leading edge of the optical pulse is as steep as a few hundred femtoseconds while the trailing edge shows exponential decay on a picosecond scale. This cross-correlation trace is consistent with the intensity autocorrelation trace without spectral filtering shown in Figure 2a.
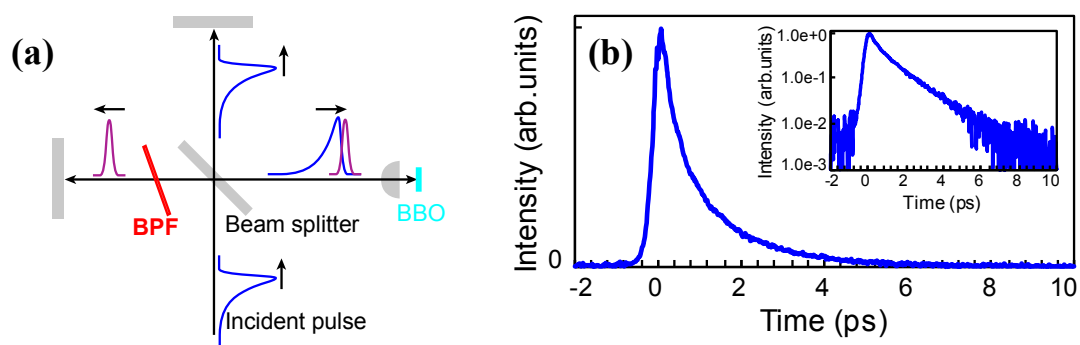

Figure 3. (**a**) Schematic representation of cross-correlation measurement. BPF: Bandpass filter, BBO: β-BaB$_2$O$_4$ crystal; (**b**) Cross-correlation measurement trace. Inset: Cross-correlation trace in logarithmic intensity scale.

We carried out further cross-correlation measurements in order to determine the time delay between spectral components at different wavelengths. We inserted another BPF into the other interferometer arm for this purpose, as shown in Figure 4a. The incidence angle for one BPF was fixed to pass a spectral component at a particular wavelength, whereas that for the other BPF was varied to extract spectral components at different wavelengths. Figure 4b shows the spectral components used for the cross-correlation analysis. These spectra were measured by introducing the optical pulses before the β-BBO crystal into the optical spectrum analyzer. Figure 4c shows the cross correlation between the spectral component at 402.3 nm and those at other wavelengths.

The peaks in the cross-correlation traces are seen to be more delayed and the traces become broader as the wavelength increases. The peak intensity of the traces slightly increases from 402.3 nm to 403.0 nm with the increase in the corresponding spectral components because the cross-correlation traces are not much broadened. For the spectral components longer than 403.3 nm, however, the peak intensity of the cross-correlation traces decreases despite the increase

in the intensity of the corresponding spectral components. This is due to the broadening of the cross-correlation traces.
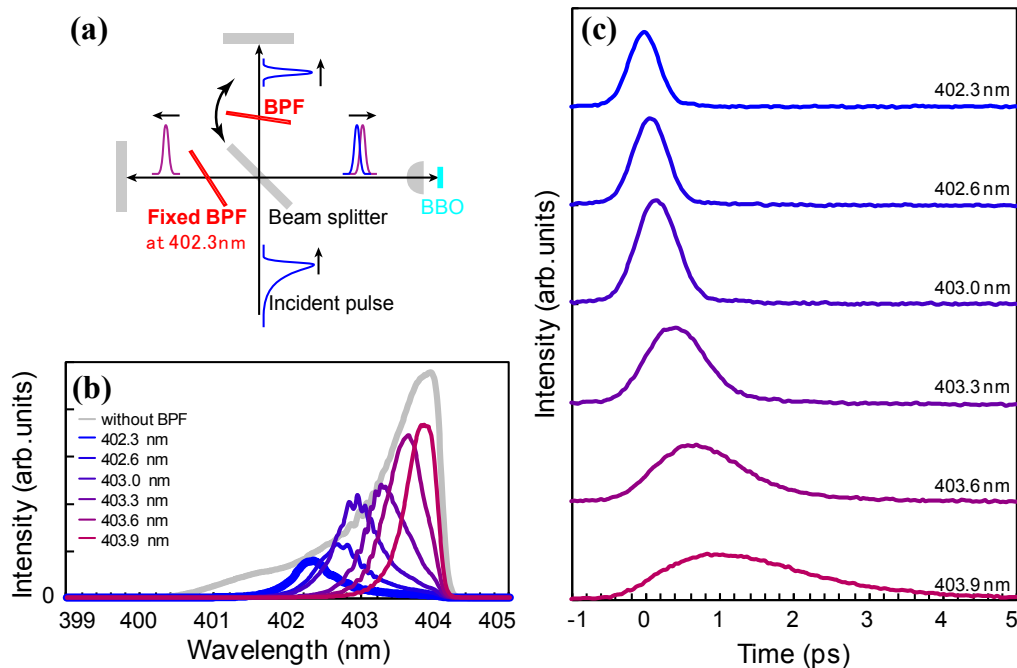

Figure 4. (**a**) Schematic representation of cross-correlation measurement setup to measure the correlation between spectral components at different wavelengths; (**b**) Spectra for cross-correlation measurement. The thick blue trace is the spectrum after the fixed BPF. The additional traces are spectra after the other BPF at different transmission wavelength. The gray trace represents the entire spectrum before the BPF. The wavelength is different from Figure 2b since the MLLD configuration is not the same; (**c**) Cross-correlation signals between the fixed spectral component at 402.3 nm and other spectral components.

Figure 5 shows the time delay of the cross-correlation peaks as a function of the wavelength. The dashed line in the figure represents the group delay due to the intracavity dispersion-compensation optics. The time delay of the cross-correlation peaks is mainly determined by the intracavity GVD. Thus, the exponential decay of the trailing edge of the optical pulses can be attributed to the time delay and to pulse broadening of the spectral components at longer wavelengths.
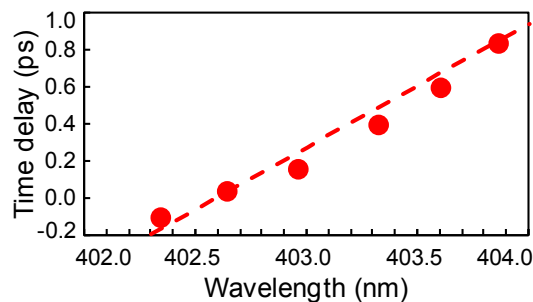

Figure 5. Delay between the spectral components measured in the cross-correlation signal shown in Figure 4c as a function of the wavelength. The dashed line represents the time delay introduced by the intracavity dispersion-compensation optics.

3.3. Spectrally-Resolved Intensity Autocorrelation Measurements

The cross-correlation results show that the picosecond-order exponential decay of the optical pulses can be attributed to the group delay due to the dispersion compensation optics, and to pulse broadening. However, the broadening of the cross-correlation trace cannot be explained only by the effects of the dispersion-compensation optics. Thus, we measured intensity autocorrelations for different spectral components with a spectral bandwidth narrower than that in our previous report [11]. Figure 6 shows optical spectra measured after the BPF, where the different transmission wavelength was changed by varying the incidence angle. The figure also shows the corresponding autocorrelation traces. As the cross-correlation traces in Figure 4c become broader with the increase in the wavelength, the pulse duration in Figure 6b increases with increasing transmission wavelength. The typical peak power of the optical pulses after the BPF was about 1.2 W at 398.8 nm, 3.0 W at 400.3 nm and 3.0 W at 401.0 nm. The resulting time-bandwidth product is plotted in Figure 7 as a function of wavelength. At wavelengths of about 399–400 nm, the time-bandwidth product is about 0.4, close to the Fourier-transform limited value, but it increases rapidly at wavelengths longer than 400 nm. The femtosecond optical pulses shown in Figure 2a obtained by spectral filtering correspond to the spectral region with the minimum time-bandwidth products.
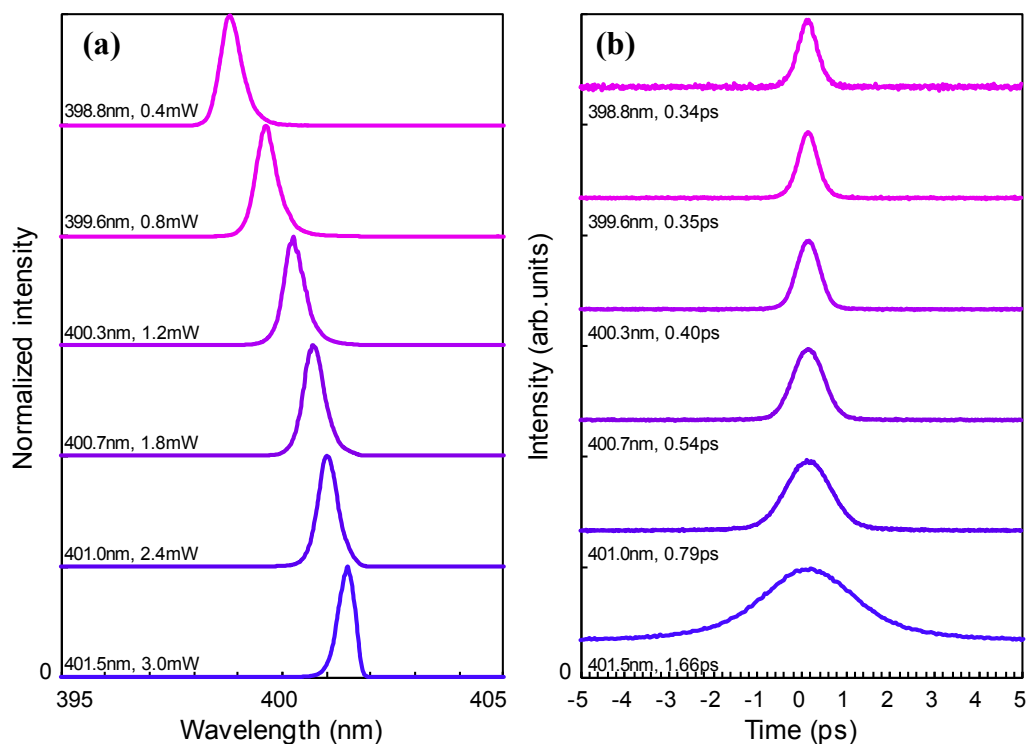

Figure 6. (**a**) Spectral components after the BPF with different transmission wavelengths and average power after the BPF; (**b**) Intensity autocorrelation traces corresponding to the spectral components after the BPF with pulse durations assuming sech^2 pulse shape.
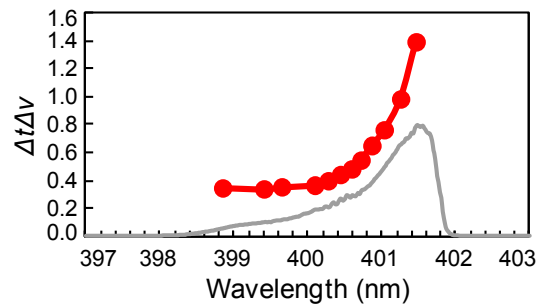
Figure 7. Time-bandwidth product of the optical pulses shown in Figure 6 as a function of the peak wavelength of the spectral components. Gray trace: the entire spectrum after the GaInN MLLD without the BPF.

3.4. Discussions

The time-bandwidth products in Figure 7 show that in the short wavelength region of the optical spectrum, there is a balance between optical nonlinearity and the negative intracavity GVD. In semiconductors, nonlinear optical effects are associated with photons with energies either below or above the band-gap energy. The former are instantaneous nonlinearities such as the Kerr effect. In semiconductor laser diodes, the cladding layers are transparent at the lasing wavelength so that the Kerr nonlinearity can occur. However, the nonlinear refractive index of GaN for photons with energies just below the band-gap energy has been reported to be large but negative [16]. This is due to the large two-photon absorption coefficient for photons close to the band-gap energy [17]. Therefore, a negative nonlinear refractive index is expected in the cladding layers, so that we consider that the instantaneous optical nonlinearity cannot balance the negative intracavity GVD in the GaInN MLLD.

The other type of optical nonlinearity to be considered is saturation in the GaInN BS-LD. In the SA and gain sections, saturation leads to the opposite sign of change in the refractive index. In the gain section, the refractive index increases with decreasing carrier density during pulse propagation. In contrast, in the SA section, the refractive index decreases as the absorption saturates [18]. Because the frequency shift increases with the degree of absorption saturation [19], this can balance the negative intracavity GVD. In the model of the saturation dynamics [19], the nonzero phase-relaxation time of the SA, T_2, was not included assuming that pulse durations were longer than T_2. The carrier-carrier scattering time in GaN is reported to be less than 15 fs [20], so that the saturation dynamics in the SA can be applied to explain the frequency shift. From Figure 7, the width of the spectral region with the minimum time-bandwidth product is as large as about 2 THz. Since the absorption coefficient for the GaInN active layer has been reported to be larger than that for other semiconductors, the large frequency shift can be inherent to GaN-based materials [12].

After the steep leading edge is formed, the gain saturation can mainly contribute to the trailing edge of the optical pulses. Since gain saturation is accompanied by carrier depletion, the refractive index increases. The temporal change in the gain is characterized by the carrier lifetime and the carrier depletion due to the stimulated emission [21]. The optical pulses from the GaInN MLLD are considered to be much shorter than the sub-ns carrier lifetime, so that the trailing edge is formed by the spectral components that are red-shifted due to the gain saturation and are delayed due to the negative intracavity GVD. This can be a reason why the peak position in Figure 5 follows the time delay of the

dispersion compensation optics. Temporal-broadening of the spectral components is more significant at longer wavelengths, as shown in Figure 6, due to the accumulation of these effects. This broadening behavior can also explain the asymmetric shape of the optical spectrum in Figure 2b. The spectrally-resolved autocorrelation traces in Figure 6 do not show coherence spikes, so the entire spectrum is coherent. This is consistent with the signal-to-noise ratio of greater than 60 dB for the RF spectrum shown in Figure 4b of Reference [10].

In our previous reports, we speculated that the femtosecond pulse generation mechanism involved soliton mode-locking, because the femtosecond optical pulses were produced by a GaInN MLLD with a negative intracavity GVD and an SA with slow absorption recovery [10,11]. Based on the above analysis, pulse formation in a dispersion-compensated GaInN MLLD can be explained in terms of the saturation dynamics of the gain and SA section in the GaInN BS-LD. Thus, a soliton-like pulse formation mechanism may be involved due to the upward frequency shift of the SA. Paschotta *et al.* reported pulse formation due to soliton-like mode locking in an external-cavity surface-emitting semiconductor laser [22]. They considered the positive intracavity dispersion and nonlinear changes in the refractive index of the gain medium and the SA. In the case of a GaInN MLLD, the pulse formation mechanism is similar, but absorption saturation can be the dominant cause of the frequency shift that balances the negative intracavity GVD. The large saturation effects in the SA and gain sections are associated with the high density of states in GaN-based semiconductors.

4. Conclusions

In conclusion, we investigated the temporal characteristics of blue-violet optical pulses from a dispersion-compensated GaInN MLLD using spectrally-resolved intensity auto- and cross-correlation measurement techniques. Based on the results, the chirp characteristics of the different spectral components were categorized in time and wavelength axes. The less-chirped pulse components in the short wavelength region consisted of the pulse leading edge and the chirp-increasing components were attributed to the spectral components at longer wavelengths that formed the trailing edge of the optical pulses. These different behaviors can be, respectively, explained by saturation effects in the SA and gain sections. In particular, a strong saturation effect in the SA section can compensate a negative intracavity GVD resulting in the formation of femtosecond optical pulses. These strong saturation effects were due to the large density of state in nitride semiconductors. These saturation dynamics are therefore important for further development of ultrashort pulse lasers based on nitride semiconductors.

Author Contributions

Planning and performing the experiments: Shunsuke Kono, Rintaro Koda, and Hideki Watanabe; writing the manuscript: Shunsuke Kono; supervising the project: Noriyuki Fuutagawa and Hironobu Narui.

Conflicts of Interest

The authors declare no conflict of interest.

References

1. Denk, W.; Strickler, J.H.; Webb, W.W. Two-Photon Laser Scanning Fluorescence Microscopy. *Science* **1990**, doi:10.1126/science.2321027.
2. Chichkov, B.N.; Momma, C.; Nolte, S.; von Alvensleben, F.; Tünnermann, A. Femotsecond, picosecond and nanosecond laser ablation of solids. *Appl. Phys. A* **1996**, doi:10.1007/BF01567637.
3. Balzer, J.C.; Schlauch, T.; Klehr, A.; Erbert, G.; Hofmann, M.R. All semiconductor high power fs laser system with variable repetition rate. *Proc. SPIE* **2012**, doi:10.1117/12.907953.
4. Amano, H.; Kito, M.; Hiramitsu, K.; Akasaki, I. P-Type Conduction in Mg-Doped GaN Treated with Low-Energy Electron Beam Irradiation (LEEBI). *Jpn. J. Appl. Phys.* **1989**, doi:10.1143/JJAP.28.L2112.
5. Nakamura, S.; Senoh, M.; Nagahama, S.; Iwasa, N.; Yamada, T.; Matsushita, T.; Kiyoku, H.; Sugimoto, Y. InGaN-Based Multi-Quantum-Well-Structure Laser Diodes. *Jpn. J. Appl. Phys.* **1996**, doi:10.1143/JJAP.35.L74.
6. Koda, R.; Oki, T.; Kono, S.; Miyajima, T.; Watanabe, H.; Kuramoto, M.; Ikeda, M.; Yokoyama, H. 300 W Peak Power Picosecond Optical Pulse Generation by Blue-Violet GaInN Mode-Locked Laser Diode and Semiconductor Optical Amplifier. *Appl. Phys. Express* **2012**, doi:10.1143/APEX.5.022702.
7. Koda, R.; Takiguchi, Y.; Kono, S.; Watanabe, H.; Hanzawa, Y.; Nakajima, H.; Shiozaki, M.; Sugawara, N.; Kuramoto, M.; Hironobu, N. Generation of a 2.2 nJ picosecond optical pulse with blue-violet wavelength using a GaInN master oscillator power amplifier. *Appl. Phys. Lett.* **2015**, doi:10.1063/1.4927641.
8. Rafailov, E.U.; Cataluna, M.A.; Sibbett, W.; Il'inskaya, N.D.; Zadiranov, Y.M.; Zhukov, A.E.; Ustinov, V.M.; Livshits, D.A.; Kovsh, A.R.; Ledentsov, N.N. High-power picosecond and femtosecond pulse generation from a two-section mode-locked quantum-dot laser. *Appl. Phys. Lett.* **2005**, doi:10.1063/1.2032608.
9. Schlauch, T.; Balzer, J.C.; Klehr, A.; Erbert, G.; Tränkle, G.; Hofmann, M.R. Femtosecond passively modelocked diode laser with intracavity dispersion management. *Opt. Express* **2010**, doi:10.1364/OE.18.024316
10. Kono, S.; Watanabe, H.; Koda, R.; Miyajima, T.; Kuramoto, M. 200-fs pulse generation from a GaInN semiconductor laser diode passively mode-locked in a dispersion-compensated external cavity. *Appl. Phys. Lett.* **2012**, doi:10.1063/1.4747808.
11. Kono, S.; Watanabe, H.; Koda, R.; Miyajima, T.; Kuramoto, M. Passively Mode-Locked GaInN Laser Diode Generating 200 fs Optical Pulses. *Jpn. J. Appl. Phys.* **2013**, doi:10.7567/JJAP.52.08JG06.

12. Miyajima, T.; Kono, S.; Watanabe, H.; Oki, T.; Koda, R.; Kuramoto, M.; Ikeda, M.; Yokoyama, H. Saturable absorbing dynamics of GaInN multiquantum well structures. *Appl. Phys. Lett.* **2011**, doi:10.1063/1.3583456.

13. Kärtner, F.X.; Keller, U. Stabilization of solitonlike pulses with a slow saturable absorber. *Opt. Lett.* **1995**, doi:10.1364/OL.20.000016.

14. Oki, T.; Saito, K.; Watanabe, H.; Miyajima, T.; Kuramoto, M.; Ikeda, M.; Yokoyama, H. Passive and Hybrid Mode-Locking of an External-Cavity GaInN Laser Diode Incorporating a Strong Saturable Absorber. *Appl. Phys. Express* **2010**, doi:10.1143/APEX.3.032104.

15. Kono, S.; Oki, T.; Kuramoto, M.; Ikeda, M.; Yokoyama, H. Intensity Autocorrelation Measurement of 400 nm Picosecond Optical Pulses from a GaInN Mode-Locked Semiconductor Laser Diode Using Surface Second Harmonic Generation of β-BaB$_2$O$_4$ Crystal. *Appl. Phys. Express* **2010**, doi:10.1143/APEX.3.122701.

16. Huang, Y.-L.; Sun, C.-K.; Liang, J.-C.; Keller, S.; Mack, M.P.; Mishra, U.K.; DenBaars, S.P. Femtosecond Z-scan measurement of GaN. *Appl. Phys. Lett.* **1999**, doi:10.1063/1.125376.

17. Sheik-Bahae, M.; Hutchings, D.C.; Hagan, D.J.; Van Stryland, E.W. Dispersion of Bound Electronic Nonlinear Refraction in Solids. *IEEE J. Quantum Electron.* **1991**, doi:10.1109/3.89946.

18. Derickson, D.J.; Helkey, R.J.; Mar, A.; Karin, J.R.; Wasserbauer, J.G.; Bowers, J.E. Short Pulse Generation Using Multisegment Mode-Locked Semiconductor Lasers. *IEEE J. Quantum Electron.* **1992**, doi:10.1109/3.159527.

19. Miranda, R.S.; Jacobovitz, G.R.; Cruz, C.H.B.; Scarparo, M.A.F. Positive and negative chirping of laser pulses shorter than 100 fsec in a saturable absorber. *Opt. Lett.* **1986**, doi:10.1364/OL.11.000224.

20. Hughes, S.; Kobayashi, T. Ultrafast carrier-carrier scattering in wide-gap GaN semiconductor laser devices. *Semicond. Sci. Technol.* **1997**, doi:10.1088/0268-1242/12/6/015.

21. Olsson, N.A.; Agrawal, G.P. Spectral shift and distortion due to self-phase modulation of picosecond pulses in 1.5 μm optical amplifiers. *Appl. Phys. Lett.* **1989**, doi:10.1063/1.101742.

22. Paschotta, R.; Häring, R.; Garnache, A.; Hoogland, S.; Tropper, A.C.; Keller, U. Soliton-like pulse-shaping mechanism in passively mode-locked surface-emitting semiconductor lasers. *Appl. Phys. B* **2002**, doi:10.1007/s00340-002-1014-5.